

Record High Magnetic Anisotropy in Chemically Engineered Iridium

Dimer

Xiaoqing Liang^{1,3}, Xue Wu¹, Jun Hu^{2,*}, Jijun Zhao^{1,*}, Xiao Cheng Zeng^{3,4*}

¹Key Laboratory of Materials Modification by Laser, Ion and Electron Beams (Dalian University of Technology), Ministry of Education, Dalian 116024, China

²College of Physics, Optoelectronics and Energy, Soochow University, Suzhou, Jiangsu 215006, China

³Department of Chemistry, University of Nebraska, Lincoln, NE 68588, USA

⁴Collaborative Innovation Center of Chemistry for Energy Materials, University of Science and Technology of China, Hefei 230026, China

Abstract

Exploring giant magnetic anisotropy in small magnetic nanostructures is of both fundamental interest and technological merit for information storage. To prevent spin flipping at room temperature due to thermal fluctuation, large magnetic anisotropy energy (MAE) over 50 meV in magnetic nanostructure is desired for practical applications. We chose one of the smallest magnetic nanostructures — Ir₂ dimer, to investigate its magnetic properties and explore possible approach to engineer the magnetic anisotropy. Through systematic first-principles calculations, we found that the Ir₂ dimer already possesses giant MAE of 77 meV. We proposed an effective way to enhance the MAE of the Ir₂ dimer to 223 ~ 294 meV by simply attaching a halogen atom at one end of the Ir-Ir bond. The underlying mechanism for the record high MAE is attributed to the modification of the energy diagram of the Ir₂ dimer by the additional halogen-Ir bonding, which alters the spin-orbit coupling Hamiltonian and hence the magnetic anisotropy. Our strategy can be generalized to design other magnetic molecules or clusters with giant magnetic anisotropy.

Keywords: Ir₂ dimer, Magnetic anisotropy, Magnetic nanostructure, Spin-orbit coupling

*Corresponding authors. Email: jhu@suda.edu.cn (J. H); zhaojj@dlut.edu.cn (J.Z); xzeng1@unl.edu (X.C.Z).

The continuous miniaturization of the spintronics devices for modern technologies such as magnetic data storage would eventually reach the ultimate length scale (i.e. one to a few atoms) [1-6]. Recently, reading and writing quantum magnetic states in magnetic nanostructures with only a few transition-metal atoms were achieved by several experimental groups [1-7]. These investigations demonstrate the fascinating possibility to utilize magnetic nanostructure and even single atom in the nanometer-scale spintronics devices. In this realm, the magnetic anisotropy of a magnetic nanostructure is the critical factor because it prevents the random spin reorientation induced by thermal fluctuation. Therefore, large magnetic anisotropic energy (MAE) is desired in magnetic nanostructures that serve as the building blocks of spintronics devices. Typical magnetic nanostructures based on 3d transition-metal (TM) atoms have MAEs of only a few meV which corresponds to a blocking temperature (T_B) under 50 K, implying that their magnetic states are stable only at very low temperature [2,8]. For practical applications of the magnetic nanostructures at room temperature, large MAEs up to about 30 ~ 50 meV are necessary.

The magnetic anisotropy of a magnetic nanostructure originates from the spin-orbit coupling (SOC) effect. By analysis of the SOC Hamiltonian based on the second-order perturbation theory, Wang *et al.* expressed the MAE as the competition between the angular momentum matrix elements $\langle L_z \rangle$ and $\langle L_x \rangle$ [9,10]:

$$MAE \approx \xi^2 \sum_{u\alpha, o\beta} (2\delta_{\alpha\beta} - 1) \left[\frac{\langle u\alpha | L_z | o\beta \rangle^2}{E_{u\alpha} - E_{o\beta}} - \frac{\langle u\alpha | L_x | o\beta \rangle}{E_{u\alpha} - E_{o\beta}} \right] \quad (1)$$

Here ξ is the SOC constant; $E_{u\alpha}$ and $E_{o\beta}$ are the energy levels of the unoccupied states with spin α ($|u\alpha\rangle$) and the occupied states with spin β ($|o\beta\rangle$), respectively. Therefore, the keys to achieve large MAE are: (i) large SOC constant ξ which exists in heavy elements such as 5d TM elements; (ii) specific energy diagram to reduce the denominator in Eq. (1) that can be realized by appropriate ligand field. For example, a large MAE of 9 meV in a single Co atom was induced by placing it on Pt(111) substrate [11], while the MAE per atom in hcp Co solid is only 0.045 meV

[12]. On the other hand, a giant MAE of 60 meV for Co adatom on MgO(001) surface was observed in a recent experiment, and such giant MAE was attributed to the special ligand field of the substrate [4]. Interestingly, combining the effects of the ligand field, orbital multiplet, and large SOC constants, even larger MAEs of 110 meV and 208 meV for Ru and Os adatom on MgO(001) surface were predicted based on density functional theory (DFT) calculations [13]. Recently, attempts to attain large MAEs with 4*f* TM elements such as Dy, Ho and Er on substrate were also made [14-16]. Despite of the large SOC constants for these 4*f* TM elements, the resulting MAEs are relatively small, i.e., 21.4 meV for Dy on graphene, 5.3 meV and 3.9 meV for Er and Ho atom on Pt(111), respectively.

In addition to the single TM adatom on specific substrate, TM dimers are of particular interest [17-21] due to their special symmetry. A homo-nuclear TM dimer is rotationally invariant around the molecular axis. Consequently, its magnetic anisotropy would arise at the first-order perturbation treatment of SOC interaction and therefore can be anomalously large compared to most other magnetic nanostructures [17]. In fact, appreciable MAEs of 30 ~ 70 meV were predicted theoretically for some free-standing TM dimers (positive MAE means easy axis parallel to the dimer axis) [20,22,23].



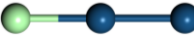


Intuitively, the energy diagram of a given TM dimer can be modified effectively by chemical functionalization, which can in turn affect the magnetic anisotropy as clearly shown in Eq. (1). Therefore, it is tempting to explore feasible ways to enhance the magnetic anisotropy of TM dimers. Besides placing the TM dimer on substrate, one possible tactic is to attach a light non-metal atom which can form strong chemical bond with the metal atom(s) (thus affect the energy diagram), yet still retain the spin moment of the entire cluster. Here, we choose Ir₂ dimer as a prototype to explore the possibility of engineering its magnetic anisotropy since Ir₂ possesses the largest MAE (70 meV) among free-standing homonuclear TM dimers [20]. Our first-principles calculations demonstrate that record high MAE up to 294 meV can be achieved in the Ir₂ dimer functionalized with a halogen atom (F, Cl, Br, I). To our knowledge, such a giant MAE is greater than any MAE value reported for small magnetic clusters in the

literature, and is thus of great potential for application in spintronics devices.

We constructed various structures for Ir_2X (X is non-metal anion atom, including F, Cl, Br, I) with X atom being located at different positions, including linear and noncollinear configurations to guarantee a complete sampling of the potential energy surface of the clusters. The structural relaxations and electronic structure calculations were carried out with spin-polarized local density approximation (LDA) in the Ceperley-Alder scheme [24,25], as implemented in OpenMX package [26]. To determine the MAEs and orbital magnetic moments, self-consistent calculations with inclusion of SOC effect were performed. The MAEs of the linear configurations for both Ir_2 dimer and Ir_2X trimers are defined as the difference between the total energies with the magnetization parallel ($E(\parallel)$) and perpendicular ($E(\perp)$) to the Ir-Ir bond direction: $MAE = E(\parallel) - E(\perp)$.

Firstly, we calculate the structural and magnetic properties of Ir_2 dimer as given in Table 1. The equilibrium Ir-Ir bond length is 2.24 Å, slightly shorter than the experimental value (2.27 Å) [27], but close to a previously computed value based on the DFT/PW91 method (2.22 Å) [20]. The binding energy is 5.4 eV, significantly larger than the experimental measurement (3.5 eV) [28] but agrees with previous calculation based on the LDA method with LanL2DZ-BSSSE basis set correction (5.5 eV) [29]. It is known that LDA tends to lead over-binding for metal clusters. Qualitatively, the large binding energy reflects the strong interaction between the two Ir atoms. The computed spin moment (M_S) is 4 μ_B without considering the SOC effect. With considering the SOC, the M_S reduces slightly to 3.86 μ_B while a large orbital moment (M_L) of 2.06 μ_B is induced, in line with previous calculation [20]. The MAE is 77 meV with easy axis parallel to the molecular axis. The present MAE is slightly larger than that reported previously (70 meV) [20], probably due to different choice of DFT methods (e.g., exchange-correlation functional and basis set).

Table 1. The ground state geometry, interatomic distance along easy-axis (d), total binding energy (E_b), spin moment (M_S), orbital moment (M_L), and magnetic anisotropy energy (MAE) for Ir_2 and Ir_2X ($\text{X}=\text{F}, \text{Cl}, \text{Br}, \text{I}$) clusters. The interatomic distances are shown as Ir-Ir (Ir-X) bond lengths for Ir_2X . The positive MAE indicates easy axis parallel to the molecular axis. The record high MAE value is highlighted in bold.

	Geometry	d (Å)	E_b (eV)	M_S (μ_B)	M_L (μ_B)	MAE (meV)
Ir_2		2.24	5.4	3.86	2.06	77
Ir_2F		2.23 (1.87)	10.7	3.02	0.98	232
Ir_2Cl		2.24 (2.19)	9.5	3.04	0.98	223
Ir_2Br		2.24 (2.31)	9.3	3.03	0.98	294
Ir_2I		2.24 (2.49)	8.8	3.01	0.99	228

To understand the origin of the novel magnetic characteristic of Ir_2 , the energy diagram of its molecular orbitals is plotted in Figure 1(a). Due to the rotational symmetry of Ir_2 dimer, the Ir-5d orbitals split into three groups: d_{xy/x^2-y^2} , $d_{xz/yz}$ and d_{z^2} . The basal plane of d_{xy/x^2-y^2} is perpendicular to the Ir-Ir bond, and those of $d_{xz/yz}$ and d_{z^2} are crossing the Ir-Ir bond. Consequently, the interaction between the two Ir atoms results in three types of hybridizations: $d_{xy/x^2-y^2} - d_{xy/x^2-y^2}$, $d_{xz/yz} - d_{xz/yz}$, and $d_{z^2} - d_{z^2}$. The corresponding bonding and antibonding states (i.e. six molecular orbitals in each spin channel) can be thus notated as δ_d/δ_d^* , π_d/π_d^* and σ_d/σ_d^* . Based on the spatial wave functions in Figure 1(b) and the spin-polarized projected density of states (PDOS) in Figure 2(a) of these molecular orbitals, we identified the characters of the energy levels and marked them in the

energy diagram in Figure 1(a). Clearly, the hybridization between the two d_{z^2} orbitals of the two Ir atoms is much stronger than those between the other orbitals. This leads to large separation in energy between σ_d and σ_d^* . The interaction between the two d_{xy/x^2-y^2} orbitals is weakest, thus the separation of their energy levels is smallest. In majority spin channel, all these molecular orbitals are occupied. In minority spin channel, the doubly degenerate δ_d^* orbital is half occupied, and π_d^* and σ_d^* are unoccupied. Therefore, the electronic configuration of these molecular orbitals is $(\sigma_d)^2(\pi_d)^4(\delta_d)^4(\delta_d^*)^3(\pi_d^*)^2(\sigma_d^*)^1$. On the other hand, the interaction between the Ir- s orbitals is also strong, and the antibonding-state molecular orbitals (σ_s^*) in both spin channels are unoccupied, resulting in an electronic configuration $(\sigma_s)^2(\sigma_s^*)^0$. In addition, there is moderate hybridization between d_{z^2} and s orbitals, as shown in Figure 2(a). Note that the electronic configuration of an isolated Ir atom is $(5d)^7(6s)^2$. Accordingly, we can conclude that each Ir-6s orbital donates one electron to Ir-5d orbitals. As a result, the total spin moment of Ir₂ is 4 μ_B , contributed by δ_d^* (1 μ_B), π_d^* (2 μ_B), and σ_d^* (1 μ_B), respectively. With inclusion of the SOC effect, the doubly degenerate δ_d^* orbital in the minority spin channel splits significantly (by ~0.9 eV) for the easy-axis magnetization, while the hard-axis magnetization does not change the energy diagram much. Furthermore, the spin and orbital moments possess large anisotropy. As seen in Table S1 of Supplemental Material, the spin moments along the easy and hard axis are 3.86 and 3.28 μ_B , while the corresponding orbital moments are 2.06 and 1.16 μ_B , respectively. Intuitively, the combined effects of large SOC splitting of δ_d^* in the minority spin channel and the large anisotropy of the spin and orbital moments are responsible for the large MAE of Ir₂ [17].

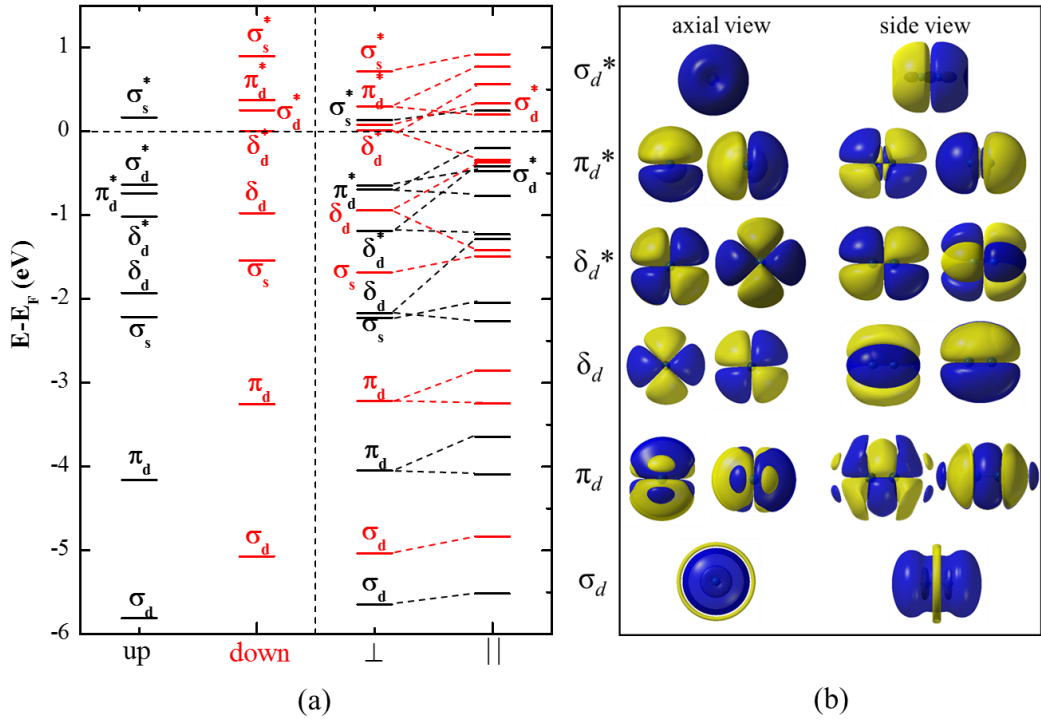


Figure 1. (a) Energy diagram of the molecular orbitals of the Ir₂ dimer without (left panel) and with (right panel) considering the SOC effect. Black refers to majority spin-up channel while red refers to minority spin-down channel. Both the magnetizations perpendicular (\perp) and parallel (\parallel) (easy axis) to the Ir-Ir bond were considered. SOC induced splitting of degenerated orbitals are denoted by the branched dashed lines. (b) The spatial wave functions of the molecular orbitals without considering the SOC effect. The paratactic orbitals are energetically degenerate. Yellow and blue correspond to different phases of the molecular wave functions, and the cutoff value of the isosurfaces is ± 0.02 a.u.

To further elucidate the underlying mechanism of the large MAE of Ir₂, we estimated the MAE of Ir₂ by using Eq. (1) to distinguish the contributions from different angular momentum matrices to the MAE. For convenience, we divide the total MAE into three parts: $MAE = MAE_{uu} + MAE_{dd} + MAE_{ud}$. These three terms are due to the coupling between the majority spin states (uu), the minority spin states (dd), and cross-spin states (ud), respectively. Since the s orbital is not involved in the SOC,

the MAE is determined by the molecular orbitals from the Ir-5d states only. From the energy diagram in Figure 1(a) and the PDOS in Figure 2(a), the Ir-5d related molecular orbitals in the majority spin channel are completely occupied, thus MAE_{uu} is negligible. For MAE_{dd} and MAE_{ud} , the nonzero contributions from the angular momentum matrix elements in Eq. (1) are plotted in Figure 2(b). Clearly, for MAE_{dd} , the contribution from L_z is much larger than that from L_x , resulting in a positive MAE_{dd} ($\sim 10\xi^2$). For cross-spin coupling, L_z still contributes more to MAE_{ud} than L_x , but this leads to a negative MAE_{ud} ($\sim -3\xi^2$) due to the negative sign in Eq. (1). Nevertheless, the absolute magnitude of MAE_{dd} is larger than that of MAE_{ud} , resulting in a positive total MAE (about $7\xi^2$) for Ir₂. Furthermore, it can be seen from Figure 2(b) that both the sign and magnitude of MAE_{dd} and MAE_{ud} are dominated by the L_z matrix elements that are related to the δ_d and δ_d^* orbitals: $\langle \delta_d, \downarrow | L_z | \delta_d^*, \downarrow \rangle$ ($\sim 17\xi^2$), $\langle \delta_d, \uparrow | L_z | \delta_d^*, \downarrow \rangle$ ($\sim 8\xi^2$) and $\langle \delta_d^*, \uparrow | L_z | \delta_d^*, \downarrow \rangle$ ($\sim 16\xi^2$). Therefore, the MAE of the Ir₂ dimer is mainly attributed to the SOC effect associated with the d_{xy/x^2-y^2} orbitals.

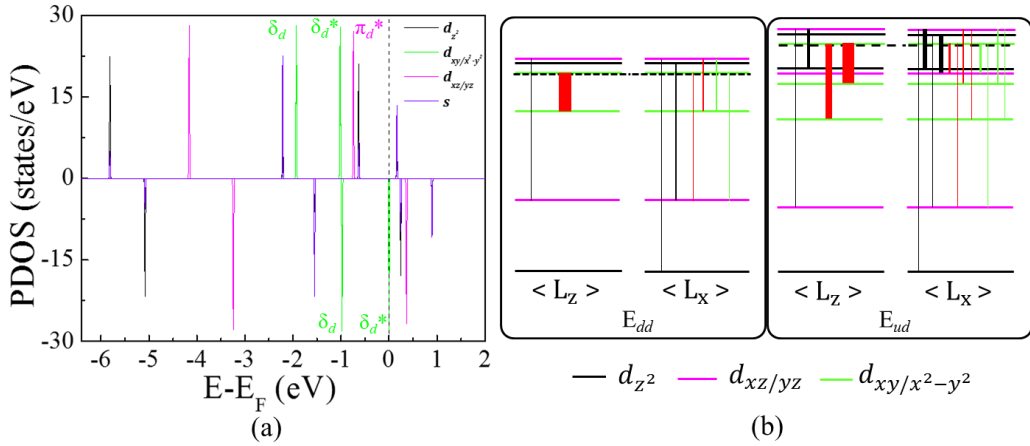


Figure 2. (a) Projected density of states (PDOS) of the s and d orbitals of Ir₂ dimer. The vertical dashed line marks the Fermi level (E_F). (b) Sketches of the nonzero contribution from each pair of molecular orbitals to the MAE between minority spin states (left panel marked as E_{dd}) and cross-spin states (right panel marked as E_{ud}). The horizontal dashed line shows the position of E_F for each case. The thickness of each

vertical line scales with the magnitude of the corresponding SOC matrix element and colors are used to distinguish different contribution from a pair of states.

According to the discussions above and Eq. (1), if an effective way to modify the energy diagram can be found, then the contribution from each pair of the molecular orbitals may be revised, thereby altering the total MAE. One such an effective tactic is by attaching an additional anion atom to Ir₂ to tailor the interaction between the two Ir atoms and the magnetic property of Ir₂. To this end, we examined a series of non-metal anion atom X, including C, Si, N, P, O, S, and halogen elements, to construct Ir₂X clusters. As shown in Tables S2 and S3, there are three types of possible equilibrium structures: (I) linear chain with X atom at one end; (II) isosceles triangle with X atom over the middle point of the Ir-Ir bond; (III) linear chain with X atom at the middle point. We obtained the ground-state structure and MAE for all the Ir₂X clusters and found that only the halogen atoms can result in huge MAEs. Hereafter, we only take the halogen elements as a prototype to discuss the strategy of chemical engineering the MAE of transition metal dimer.

For all halogen elements X (X = F, Cl, Br, I), the Ir₂X clusters prefer type-I structure (see Table S3 in Supplemental Material). As seen from Table 1, the Ir-Ir bond length in Ir₂X is slightly changed by X, while the Ir-X bond length increases monotonically with X for X = F to I due to the increasing atomic radius. Moreover, the binding energies of the Ir₂X trimers are about twice of that of Ir₂, indicating high structural stability of the entire trimer and strong binding between Ir and X atoms. Consequently, the interaction between the two Ir atoms is significantly modified, as manifested by the PDOS of Ir₂F, as an example, in Figure 3(a). It can be seen that the F-2*p* orbitals hybridize strongly with the $d_{xz/yz}$ and d_{z^2} orbitals of the Ir1 atom (bonded with X). Compared to those of Ir₂, the bonding states of both $d_{xz/yz}$ and d_{z^2} orbitals of the Ir1 atom shift downward by about 0.3 eV in the majority spin channel and 0.6 eV in the minority spin channel, while the antibonding states of $d_{xz/yz}$ and d_{z^2} shift upward by about 0.7 eV and 0.3 eV, respectively. As a result,

the hybridization between the two Ir atoms through the $d_{xz/yz}$ and d_{z^2} orbitals is markedly weakened. The energy levels of the $d_{xz/yz}$ and d_{z^2} orbitals of the Ir2 atom (at the other end of Ir₂X) shift upwards, and the energy separations between the corresponding bonding and antibonding states become narrower. Meanwhile, some electrons are transferred from the $d_{xz/yz}$ and d_{z^2} orbitals of the Ir atoms to the F atom, as shown by the inset in Figure 3(a). On the other hand, the interaction between the d_{xy/x^2-y^2} orbitals of the Ir atoms is not affected much, but slightly weakened only. Therefore, the δ_d and δ_d^* are similar with those of Ir₂ but their energy separation is narrowed by about 0.24 eV [see Figure 3(a)]. At the same time, the exchange splitting increases by about 0.52 eV.

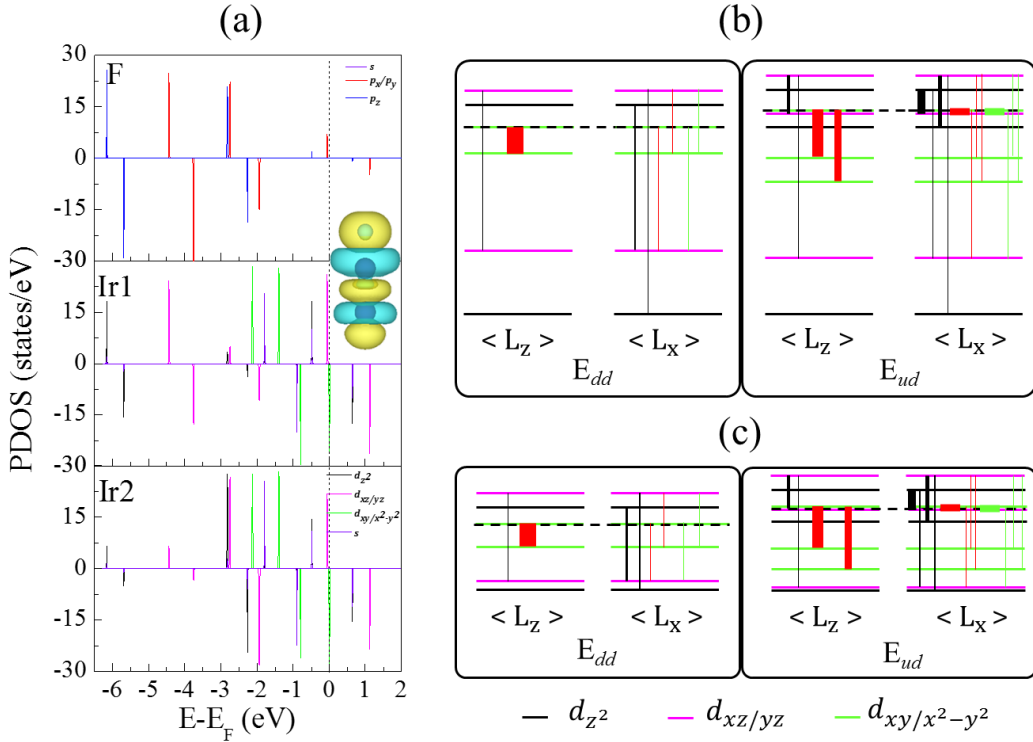


Figure 3. (a) Projected density of states (PDOS) of Ir₂F, s and p orbitals of F atom and s and d orbitals of two Ir atoms (Ir1 is the neighboring atom of F atom and Ir2 is at the end of Ir₂F) are separately shown in the panels. The insets are the corresponding charge redistribution. The yellow and blue areas refer to the electron accumulation and depletion, respectively, with isosurface value of $6 \times 10^{-3} \text{ e}/\text{\AA}^3$. The vertical dashed lines mark the Fermi level (E_F). (b, c) Sketches of the nonzero contribution from each

pair of molecular orbitals to the MAE between minority spin states (left panel marked as E_{dd}) and cross-spin states (right panel marked as E_{ud}) for the two Ir atoms of Ir_2F . The horizontal dashed line shows the position of Fermi level E_F for each case. The width of each vertical line scales with the magnitude of the corresponding SOC matrix element and the colors are used to distinguish different contribution from a pair of states.

The magnetic moments are also significantly modified by attaching X atom to the Ir_2 dimer. Without considering SOC, the total spin moments of these Ir_2X trimers are all $5 \mu_B$, larger than that of Ir_2 by $1 \mu_B$. According to the Milliken population analysis, the Ir_2 dimer donates the electron of $\delta_d^*(\downarrow)$ to the halogen atom X. Thus, the spin moment is contributed by δ_d^* ($2 \mu_B$), π_d^* ($2 \mu_B$), and σ_d^* ($1 \mu_B$). However, the SOC effect notably reduces M_S of Ir_2X to $3 \mu_B$ (see Table 1), which is even smaller than that of Ir_2 by $1 \mu_B$. On the contrary, the M_S of Ir_2 itself is only slightly altered by the SOC. From the PDOS without considering SOC (Fig. 3(a)), we can see that both $\pi_d^*(\uparrow)$ and $\delta_d^*(\downarrow)$ are very close to the E_F , which is pinned within the small gap (61 meV) between them. With considering SOC (axial magnetization), both $\pi_d^*(\uparrow)$ and $\delta_d^*(\downarrow)$ split into two orbitals, with splitting of the corresponding energy levels being as large as 498 meV and 896 meV, respectively (see Fig. S1 in Supplemental Material). Consequently, the higher energy level stemmed from $\pi_d^*(\uparrow)$ shifts upward above the E_F , while the lower energy level stemmed from $\delta_d^*(\downarrow)$ shifts downward below the E_F . One electron of $\pi_d^*(\uparrow)$ in majority spin channel transfers to $\delta_d^*(\downarrow)$ in minority spin channel, resulting in reduction of spin moment by $1 \mu_B$, i.e. the distribution of the spin moment changes to δ_d^* ($1 \mu_B$), π_d^* ($1 \mu_B$), and σ_d^* ($1 \mu_B$). In addition, the orbital moments of Ir_2X trimers are about $1 \mu_B$, which is about half of that of Ir_2 . As shown in Table S1 of Supplemental Material, both the local spin moment and orbital moment on Ir1 atom are smaller than those on Ir2 atom due to the hybridization between Ir1 and X atoms. It is worthy of noting that the orbital moments in Ir_2X trimers show very little anisotropy between the easy and hard axis, despite of the enhanced anisotropy of spin moments with respect to Ir_2 .

Remarkably, the MAEs of all Ir₂X trimers are largely enhanced (see Table 1). Among them, Ir₂Cl entails the least MAE yet the MAE value is still as large as 223 meV; Ir₂Br has the largest MAE of 294 meV; and the MAEs of the other two trimers are about 230 meV. All these MAE values are larger than the highest MAE values reported in the literature for small magnetic clusters. The largest MAE value we are aware of is 208 meV for the Os adatom on MgO(001) [13].

To confirm our view of the underlying mechanism for the extraordinary enhancement of MAE due to functionalization by halogen atoms, we extracted the energy levels from the PDOS in Figure 3(a) and estimated the MAEs of Ir₂F using Eq. (1), as plotted in Fig. 3(b) and 3(c). From the nonzero contributions of the angular momentum shown in Fig. 3(b) and 3(c), the main contributions stem from the matrix elements of L_Z ($\langle \delta_{d,\downarrow} | L_Z | \delta_{d,\downarrow}^* \rangle$, $\langle \delta_{d,\uparrow} | L_Z | \delta_{d,\downarrow}^* \rangle$, $\langle \delta_{d,\uparrow}^* | L_Z | \delta_{d,\downarrow}^* \rangle$) and L_X ($\langle \pi_{d,\uparrow}^* | L_X | \delta_{d,\downarrow}^* \rangle$) of both Ir atoms. Compared to Ir₂ (see Table S4 in Supplemental Material), the positive contribution of $\langle \delta_{d,\downarrow} | L_Z | \delta_{d,\downarrow}^* \rangle$ increases weakly and the negative contributions of $\langle \delta_{d,\uparrow} | L_Z | \delta_{d,\downarrow}^* \rangle$ and $\langle \delta_{d,\uparrow}^* | L_Z | \delta_{d,\downarrow}^* \rangle$ are slightly reduced. Interestingly, the contribution from $\langle \pi_{d,\uparrow}^* | L_X | \delta_{d,\downarrow}^* \rangle$ is minor in Ir₂ due to the relatively large energy separation between the corresponding orbitals. For Ir₂F, however, the energy levels of $\pi_{d,\uparrow}^*$ and $\delta_{d,\downarrow}^*$ become very close [~ 61 meV; see Fig. 3(a)], which results in huge contribution to MAE from $\langle \pi_{d,\uparrow}^* | L_X | \delta_{d,\downarrow}^* \rangle$. The final estimated MAE_{dd} and MAE_{ud} are $13\xi^2$ and $44\xi^2$, respectively, both being larger than the corresponding values for Ir₂ ($10\xi^2$ and $-3\xi^2$). Consequently, the total MAE of Ir₂F increases dramatically to 232 meV, about three times of that of Ir₂ (77 meV). In fact, for all Ir₂X trimers considered here, the term $\langle \pi_{d,\uparrow}^* | L_X | \delta_{d,\downarrow}^* \rangle$ dominates the MAE (see Table S4 in Supplemental Material) because they all have similar energy diagrams (see Fig. S2 in Supplemental Material).

In conclusion, our first-principles calculations demonstrate that the MAE of the Ir₂ dimer can be significantly enhanced up to a record high value of 294 meV by attaching a Br atom at one end of the Ir-Ir bond. Analysis of the energy levels and the matrix elements of the SOC Hamiltonian show that the d_{xy/x^2-y^2} and $d_{xz/yz}$

orbitals are mainly responsible for the record high MAE value. More specifically, the halogen atoms with strong electronegativity lead to the stable linear configuration for the Ir_2X trimer, and induce large spin moments. The strategy of functionalization of TM-based cluster introduces a new synthetic approach to chemically engineering the magnetic anisotropy of TM clusters towards future-generation magnetic information storages using single or a few atoms per bit.

Acknowledgements

This work was supported by the National Natural Science Foundation of China (11574040, 11574223), the Natural Science Foundation of Jiangsu Province (BK20150303), the Fundamental Research Funds for the Central Universities of China (DUT16-LAB01, DUT17LAB19), and the Supercomputing Center of Dalian University of Technology. J.H. thanks the Jiangsu Specially-Appointed Professor Program of Jiangsu Province. X.C.Z. was supported by a State Key R&D Fund of China (2016YFA0200604) to USTC and University of Nebraska Holland Computing Center.

References

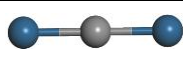
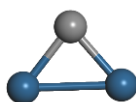

- [1] A. A. Khajetoorians, J. Wiebe, B. Chilian, and R. Wiesendanger, *Science* **332**, 1062 (2011).
- [2] S. Loth, S. Baumann, C. P. Lutz, D. M. Eigler, and A. J. Heinrich, *Science* **335**, 196 (2012).
- [3] A. A. Khajetoorians *et al.*, *Science* **339**, 55 (2013).
- [4] I. G. Rau *et al.*, *Science* **344**, 988 (2014).
- [5] T. Miyamachi *et al.*, *Nature* **503**, 242 (2013).
- [6] M. Steinbrecher, A. Sonntag, M. dos Santos Dias, M. Bouhassoune, S. Lounis, J. Wiebe, R. Wiesendanger, and A. Khajetoorians, *Nat. Commun.* **7**, 10454 (2016).
- [7] F. D. Natterer, K. Yang, W. Paul, P. Willke, T. Choi, T. Greber, A. J. Heinrich, and C. P. Lutz, *Nature* **543**, 226 (2017).
- [8] F. Meier, L. Zhou, J. Wiebe, and R. Wiesendanger, *Science* **320**, 82 (2008).
- [9] D.-s. Wang, R. Wu, and A. J. Freeman, *Phy. Rev. B* **47**, 14932 (1993).
- [10] J. Hu and R. Wu, *Phys. Rev. Lett.* **110**, 097202 (2013).
- [11] P. Gambardella *et al.*, *Science* **300**, 1130 (2003).
- [12] D. Weller and A. Moser, *IEEE Transactions on Magnetics* **35**, 4423 (1999).
- [13] X. Ou, H. Wang, F. Fan, Z. Li, and H. Wu, *Phys. Rev. Lett.* **115**, 257201 (2015).
- [14] R. Baltic, M. Pivetta, F. Donati, C. Wäckerlin, A. Singha, J. Dreiser, S. Rusponi, and H. Brune, *Nano Lett.* **16**, 7610 (2016).
- [15] F. Donati, A. Singha, S. Stepanow, C. Wäckerlin, J. Dreiser, P. Gambardella, S. Rusponi, and H. Brune, *Phys. Rev. Lett.* **113**, 237201 (2014).
- [16] F. Donati *et al.*, *Science* **352**, 318 (2016).
- [17] T. O. Strandberg, C. M. Canali, and A. H. MacDonald, *Nat. Mater.* **6**, 648 (2007).
- [18] T. O. Strandberg, C. M. Canali, and A. H. MacDonald, *Phy. Rev. B* **77**, 174416 (2008).
- [19] D. Fritsch, K. Koepernik, M. Richter, and H. Eschrig, *J. Comput. Chem.* **29**, 2210 (2008).
- [20] P. Błoński and J. Hafner, *Phy. Rev. B* **79**, 224418 (2009).
- [21] B. Piotr and H. Jürgen, *J. Phys.: Condens. Matter* **26**, 146002 (2014).
- [22] H. K. Yuan, H. Chen, A. L. Kuang, B. Wu, and J. Z. Wang, *J. Phys. Chem. A* **116**, 11673 (2012).
- [23] P. Wang, X. Jiang, J. Hu, X. Huang, and J. Zhao, *J. Mater. Chem. C* **4**, 2147 (2016).
- [24] D. M. Ceperley and B. Alder, *Phys. Rev. Lett.* **45**, 566 (1980).
- [25] J. P. Perdew and A. Zunger, *Physical Review B* **23**, 5048 (1981).
- [26] H. K. T. Ozaki, J. Yu, M.J. Han, N. Kobayashi, M. Ohfuti, F. Ishii, et al. , User's manual of OpenMX version 3.7.
- [27] M. D. Morse, *Chem. Rev.* **86**, 1049 (1986).
- [28] A. Miedema and K. A. Gingerich, *J. Phys. B: At. Mol. Phys.* **12**, 2081 (1979).
- [29] A. Posada-Borbón and A. Posada-Amarillas, *Chem. Phys. Lett.* **618**, 66 (2015).

Supplemental Material

Table S1. On-site spin moments and orbital moments (in μ_B) of Ir and X atoms along easy magnetization direction (M_S^e and M_L^e) and hard magnetization direction (M_S^h and M_L^h), respectively. Ir1 is the neighboring atom of X atom and Ir2 atom is located at the end of Ir_2X (X = F, Cl, Br, I).

	M_S^e			M_L^e			M_S^h			M_L^h		
	Ir1/Ir2	X	Total	Ir1/Ir2	X	Total	Ir1/Ir2	X	Total	Ir1/Ir2	X	Total
Ir_2	1.93/1.93	--	3.86	1.03/1.03	--	2.06	1.64/1.64	--	3.28	0.58/0.58	--	1.16
Ir_2F	1.40/1.55	0.08	3.02	0.40/0.68	-0.09	0.98	0.85/0.91	0.03	1.79	0.43/0.46	-0.02	0.86
Ir_2Cl	1.36/1.57	0.11	3.04	0.48/0.66	-0.15	0.98	0.81/0.96	0.03	1.79	0.43/0.47	-0.03	0.87
Ir_2Br	1.37/1.58	0.09	3.03	0.49/0.66	-0.16	0.98	1.62/1.80	0.12	3.55	0.49/0.52	-0.01	0.99
Ir_2I	1.38/1.58	0.05	3.01	0.52/0.66	-0.19	0.99	0.79/0.98	0.01	1.78	0.45/0.43	-0.01	0.87

Table S2. The atomic configurations and energy differences (ΔE) of Ir_2 dimer bonded with a carbon, silicon, pnictogen, or chalcogen atom. The spin moment (M_S) without inclusion of the SOC, easy magnetization direction (easy-axis) and the magnetic anisotropy energy (MAE) are listed for the ground-state structure. All results are calculated by using LDA method implemented in OpenMX package.

$\begin{matrix} X \\ \uparrow \\ \rightarrow Z \end{matrix}$	Configuration	ΔE (eV)	M_S (μ_B)	easy-Axis	MAE(meV)
Ir_2C		0	2	Z	10.9
		1.84	2	--	--
		3.20	2	--	--

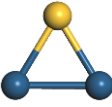
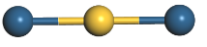
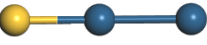
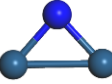
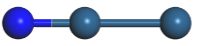
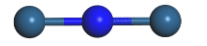

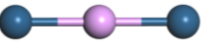
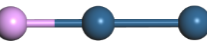

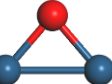
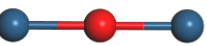
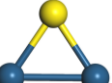
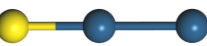
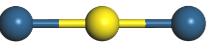
Ir ₂ Si		0	2	Y	8.8
		1.36	2	--	--
		2.63	4	--	--
Ir ₂ N		0	1	Z	2.2
		0.63	1	--	--
		1.81	1	--	--
Ir ₂ P		0	1	X	0
		1.28	1	--	--
		2.09	3	--	--
Ir ₂ O		0	0	--	--
		1.46	2	--	--
		3.42	0	--	--
Ir ₂ S		0	0	--	--
		0.23	2	--	--
		1.58	0	--	--

Table S3. The atomic configurations and energy differences (ΔE) of the metastable isomers (denoted as II and III) compared to the ground state structure (denoted as I), the bond lengths of Ir-Ir and Ir-X in the parentheses, and the total spin moments (M_S) without inclusion of the SOC.


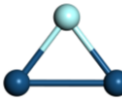
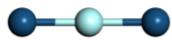
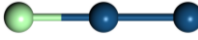
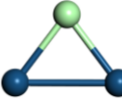
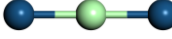

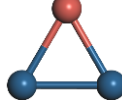
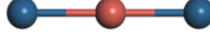
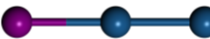
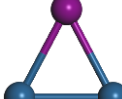

	Isomer	Configuration	d (Å)	ΔE (eV)	M_S (μ_B)
Ir ₂ F	I		2.27 (1.91)	0	5
	II		2.29 (2.19)	1.69	5
	III		-- (1.97)	4.68	5
Ir ₂ Cl	I		2.28 (2.23)	0	5
	II		2.40 (2.26)	1.01	3
	III		-- (2.15)	3.44	3
Ir ₂ Br	I		2.28 (2.35)	0	5
	II		2.39 (2.36)	0.75	3
	III		-- (2.29)	3.48	5
Ir ₂ I	I		2.28 (2.53)	0	5
	II		2.38 (2.53)	0.36	3
	III		-- (2.46)	3.31	5

Table S4. The estimated contributions of MAE based on Eq.(1), including the total MAE_{dd} and MAE_{ud}. The main contribution of MAE_{dd} from the matrix element L_Z ($\langle \delta_d, \downarrow | L_Z | \delta_d^*, \downarrow \rangle$) is listed separately, and those in the columns of MAE_{ud} are the main contributions from the matrix elements of L_Z ($\langle \delta_d, \uparrow | L_Z | \delta_d^*, \downarrow \rangle$ and $\langle \delta_d^*, \uparrow | L_Z | \delta_d^*, \downarrow \rangle$) and L_X ($\langle \pi_d^*, \uparrow | L_X | \delta_d^*, \downarrow \rangle$). All values are in unit of constant ξ^2 , where ξ is the SOC constant.

	MAE _{dd}		MAE _{ud}			
	total	$\langle \delta_d, \downarrow L_Z \delta_d^*, \downarrow \rangle$	total	$\langle \delta_d, \uparrow L_Z \delta_d^*, \downarrow \rangle$	$\langle \delta_d^*, \uparrow L_Z \delta_d^*, \downarrow \rangle$	$\langle \pi_d^*, \uparrow L_X \delta_d^*, \downarrow \rangle$
Ir ₂	10	17	-3	-8	-16	5
Ir ₂ F	13	20	44	-13	-9	49
Ir ₂ Cl	13	20	51	-13	-9	51
Ir ₂ Br	14	21	98	-12	-8	100
Ir ₂ I	12	21	220	-12	-8	222

Table S5. The spin moment (M_S) in μ_B without considering the SOC, and MAE values in meV computed based on the PBE method implemented in OpenMX, DMol³, and VASP packages, and compared to LDA results by OpenMX.

	OpenMX				VASP		DMol ³
	M_S (LDA)	MAE (LDA)	M_S (GGA)	MAE (GGA)	M_S (GGA)	MAE (GGA)	M_S (GGA)
Ir ₂	4	77	4	18	4	41	4
Ir ₂ F	5	232	5	211	5	202	5
Ir ₂ Cl	5	223	5	156	5	258	5
Ir ₂ Br	5	294	5	218	5	251	5
Ir ₂ I	5	228	5	141	5	230	5

Table S6. The Cartesian coordinates (\AA) of Ir_2 and Ir_2X ($\text{X} = \text{F}, \text{Cl}, \text{Br}, \text{I}$) clusters in the ground state structures, based on LDA-CA method implemented in OpenMX.

Cluster		x	y	z
Ir_2	Ir	0.00000	0.00000	-0.02035
	Ir	0.00000	0.00000	2.22035
Ir_2F	F	0.00000	0.00000	0.01478
	Ir	0.00000	0.00000	1.92503
	Ir	0.00000	0.00000	4.19082
Ir_2Cl	Cl	0.00000	0.00000	0.01015
	Ir	0.00000	0.00000	2.24440
	Ir	0.00000	0.00000	4.52141
Ir_2Br	Br	0.00000	0.00000	0.02207
	Ir	0.00000	0.00000	2.37409
	Ir	0.00000	0.00000	4.65362
Ir_2I	I	0.00000	0.00000	0.02347
	Ir	0.00000	0.00000	2.55427
	Ir	0.00000	0.00000	4.83460

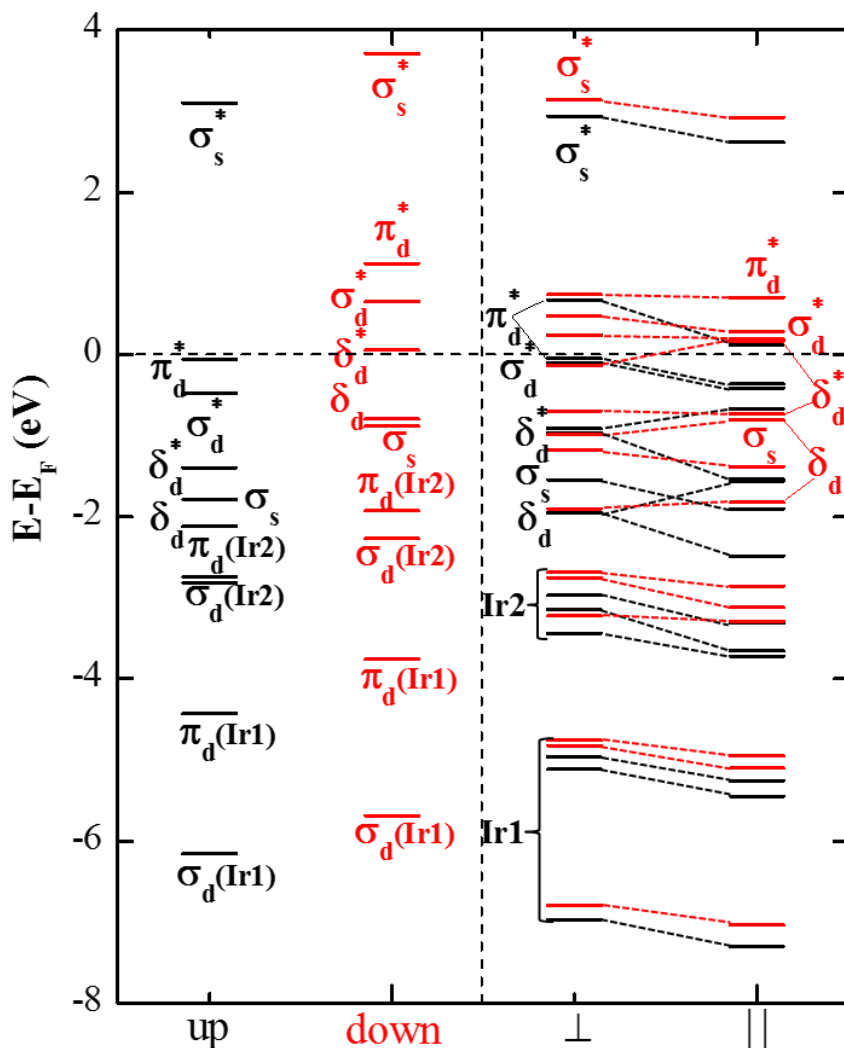


Figure S1. Energy diagram of the molecular orbitals of the Ir₂F without (left panel) and with (right panel) considering the SOC effect. Black refers to majority spin-up channel while red refers to minority spin-down channel. Both the magnetizations perpendicular (\perp) and parallel (\parallel) to the bond direction were considered. SOC induced splitting of degenerated orbitals are denoted by the branched dashed lines. The notations in the parentheses indicate that the corresponding energy levels are contributed dominantly by which Ir atom. The energy levels without such kind of notation are contributed by both Ir atoms comparably.

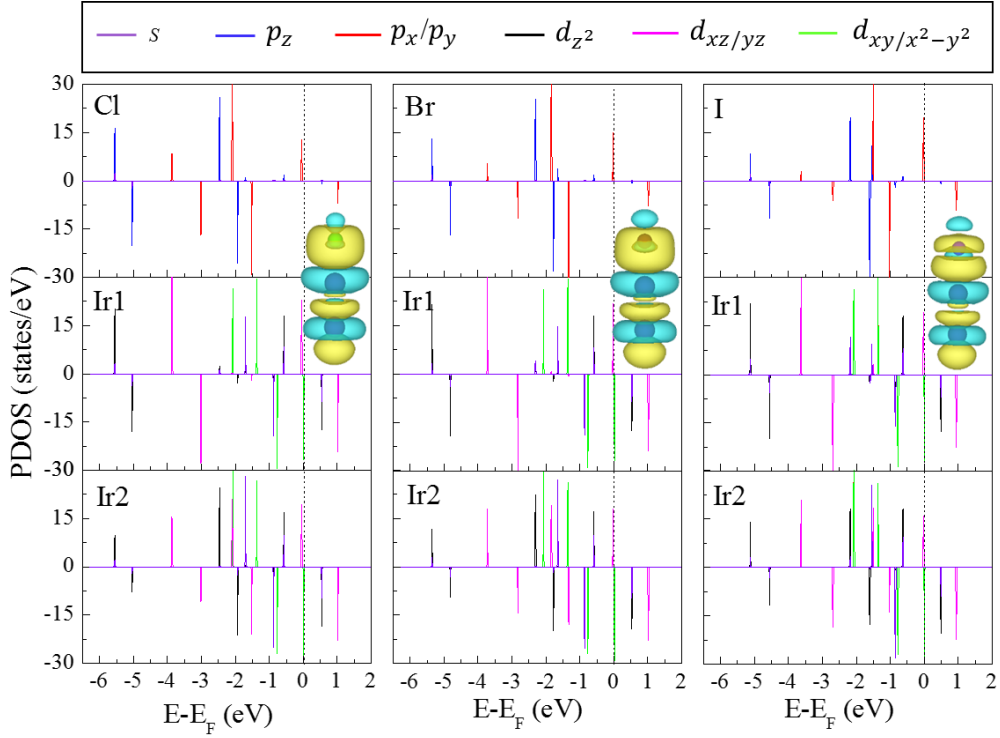


Figure S2. Projected density of states (PDOS) of Ir_2X ($\text{X} = \text{Cl}, \text{Br}, \text{I}$), s orbitals of all atoms, p orbitals of X atom and d orbitals of two Ir atoms (Ir1 is the neighboring atom of F atom and Ir2 is at the end of Ir_2F) are shown separately in the panels. The insets present the corresponding charge redistribution. The yellow and blue areas refer to the electron accumulation and depletion, respectively, with isosurface value of $6 \times 10^{-3} \text{ e}/\text{\AA}^3$.

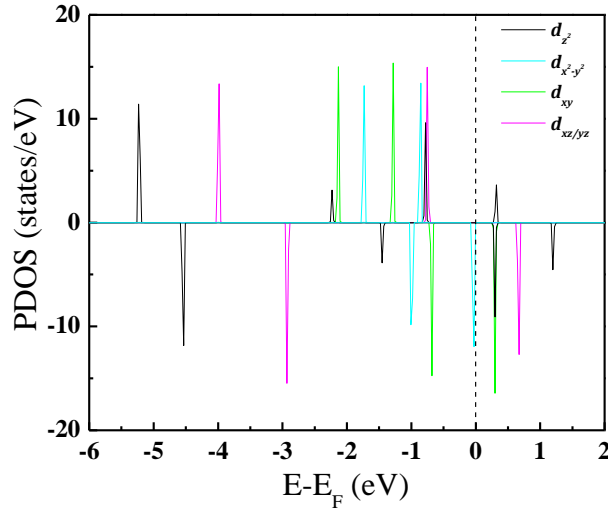


Figure S3. Projected density of states (PDOS) of the d orbitals of Ir_2 dimer from computation executed in VASP. The vertical dashed line marks the Fermi level (E_F).

Methods

We used OpenMX software package which is based on density functional theories (DFT) [1,2], norm-conserving pseudopotentials [3-7], and pseudo-atomic localized basis functions[8,9]. The cutoff radii of the radial wave function were 9.0, 7.0, 9.0, 9.0 and 11.0 a.u. and the valence orbitals were $s^2p^2d^2f^4$, $s^3p^3d^2$, $s^3p^3d^2$, $s^4p^4d^3f^4$, and $s^3p^3d^3f^2$ for Ir, F, Cl, Br and I, respectively. The fully relativistic pseudopotentials [7] were used, and the cutoff energy was set to 300 Ry. The criteria for energy and force convergence were 10^{-7} Hartree and 10^{-4} Hartree/bohr, respectively.

Justifications of different exchange-correlation functionals and different first-principles packages

In order to justify whether the LDA is reliable to describe the magnetic properties including spin moment and magnetic anisotropy energy (MAE), we used PBE functional [10] within generalized gradient approximation (GGA), implemented in OpenMX, DMol³ and VASP packages to reoptimize the structures of the Ir₂ and Ir₂X (X = F, Cl, Br, I) clusters, and compute their spin moments and MAEs accordingly. We carried out spin-polarized density functional theory calculations within GGA-PBE functional, implemented in VASP package [11,12]. The interaction between the valence electrons and ionic cores was described by the projector augmented wave (PAW) [13] method. Every individual clusters were placed in a simple cubic supercell of $20 \times 20 \times 20 \text{ \AA}^3$ to ensure sufficient separation between the periodic images. The energy cutoff for the plane-wave basis was set to 500 eV. During the self-consistent electronic structure calculations and geometry optimizations, the criteria for energy and force convergence were 10^{-6} eV and 10 meV/\AA , respectively. We defined the easy magnetization orientation aligned parallel to the bond direction as positive MAE, while perpendicular to bond direction as negative MAE, which is convenient to compare MAEs by different methods. And also we used DMol³ [14,15] to obtain the most stable magnetic state in different multiplicity, The GGA-PBE functional with basis-set of double numerical basis including *p*-polarization function are executed in DMol³ package, the cutoff radius is 6 \AA and the criteria for energy convergence is 10^{-7} Hartree during the selfconsistent electronic calculation.

For comparison, all the results calculated with different methods and first-principles packages are summarized in Table S5. First, the total spin moments for each cluster are consistent. However, the MAEs of Ir₂X calculated with GGA functional using either OpenMX or VASP are generally smaller than the values calculated with LDA in OpenMX, but still large enough to prevail most reported values in the literature. To explore the origin of MAE of a TM cluster, accurate energy levels are needed. From the calculations using different packages and different functionals, we found that only the LDA in OpenMX and GGA in DMol³ can describe the energy diagrams of Ir₂ and Ir₂X correctly, considering the constraint of the special symmetries in these clusters. Both LDA and GGA in VASP cannot produce correct energy diagrams (see Fig. S3), which implies that the approaches based on plane-waves are not suitable for studying very small clusters like Ir₂ and Ir₂X. On the other hand, DMol³ lacks the capability to calculate MAE. Hence we adopted the LDA implemented in OpenMX to calculate the structural, electronic and magnetic properties of Ir₂ and Ir₂X. As discussed in the main text, our present results on Ir₂ from LDA calculation with OpenMX agree well with previous experimental and theoretical data.

References

- [1] P. Hohenberg and W. Kohn, Physical review **136**, B864 (1964).
- [2] W. Kohn and L. J. Sham, Physical review **140**, A1133 (1965).
- [3] G. Bachelet, D. Hamann, and M. Schlüter, Phy. Rev. B **26**, 4199 (1982).
- [4] N. Troullier and J. L. Martins, Phy. Rev. B **43**, 1993 (1991).
- [5] L. Kleinman and D. Bylander, Phys. Rev. Lett. **48**, 1425 (1982).
- [6] P. E. Blöchl, Phy. Rev. B **41**, 5414 (1990).
- [7] I. Morrison, D. Bylander, and L. Kleinman, Phy. Rev. B **47**, 6728 (1993).
- [8] T. Ozaki, Phy. Rev. B **67**, 155108 (2003).
- [9] T. Ozaki and H. Kino, Phy. Rev. B **69**, 195113 (2004).
- [10] J. P. Perdew, K. Burke, and M. Ernzerhof, Phys. Rev. Lett. **77**, 3865 (1996).
- [11] G. Kresse and J. Furthmüller, Phy. Rev. B **54**, 11169 (1996).
- [12] G. Kresse and D. Joubert, Phy. Rev. B **59**, 1758 (1999).
- [13] P. E. Blöchl, Phy. Rev. B **50**, 17953 (1994).
- [14] B. Delley, J. Chem. Phys. **92**, 508 (1990).
- [15] B. Delley, J. Chem. Phys. **113**, 7756 (2000).